

To appear in the *Astronomical Journal*.

FUSE Observations of Atomic Abundances and Molecular Hydrogen in the Leading Arm of the Magellanic Stream

Kenneth. R. Sembach¹, J. Christopher Howk¹, Blair D. Savage², J. Michael Shull³

ABSTRACT

We present *Far Ultraviolet Spectroscopic Explorer* observations of the atomic and molecular absorption in high velocity cloud HVC 287.5+22.5+240, which lies in front of the ultraviolet-bright nucleus of the Seyfert 1 galaxy NGC 3783. We detect H₂, N I, N II, Si II, and Fe II and set limits on the amount of absorption due to P III, Ar I, and Fe III. We extend the earlier metallicity and dust-depletion measurements made by Lu and collaborators by examining the relative gas-phase abundances of Si, P, S, and Fe. Corrections to the derived gas-phase abundances due to ionized gas in the HVC are small ($\lesssim 15\%$). The HVC has a metallicity of 0.2–0.4 solar, similar to that of the Small Magellanic Cloud. The relative abundance pattern for the elements studied resembles that of warm gas in the SMC, which supports the idea that this HVC is part of the tidally stripped Leading Arm of the Magellanic Stream. The abundance pattern implies that the HVC contains dust grains that have been processed significantly; it is likely that the grain mantles have been modified or stripped back to expose the grain cores. We have identified more than 30 lines of H₂ arising in the HVC from rotational levels $J=0$ to $J=3$. Synthetic spectra and a curve-of-growth fit to these lines with $b = 12 \text{ km s}^{-1}$ indicate that $\log N(\text{H}_2) = 16.80 \pm 0.10$ and $f_{\text{H}_2} = 2N(\text{H}_2)/[N(\text{H I}) + 2N(\text{H}_2)] = 1.6 \times 10^{-3}$. A two-component temperature distribution is necessary to explain the observed populations of the H₂ rotational levels. We find $T_{01} = 133 \pm_{21}^{37} \text{ K}$, and $T_{23} = 241 \pm_{17}^{20} \text{ K}$, indicating that the conditions in the molecular gas are more similar to those found for diffuse molecular clouds in the Galactic halo than to those for molecular clouds in the Galactic disk. From an analysis of the $J=2$ and $J=3$ populations, we find an absorption rate (at 1000 \AA) of $\beta_{\text{uv}} < 0.1$ times the average value in the solar neighborhood. The presence of molecular gas in the HVC requires that either the H₂ formed in situ or that molecules formed within the SMC survived tidal stripping. We favor the latter possibility because of the long H₂ formation time ($\sim 10^8$ years) derived for this HVC.

¹Department of Physics & Astronomy, The Johns Hopkins University, Baltimore, MD 21218

²Department of Astronomy, University of Wisconsin, Madison, WI 53706

³CASA and JILA, Department of Astrophysical and Planetary Sciences, University of Colorado, Boulder, CO 80309

Subject headings: ISM: clouds – ISM: atoms – ISM: H II regions – Galaxy: abundances
– Galaxy: halo – ultraviolet: spectra

1. Introduction

The spatial distribution and velocities of neutral interstellar clouds moving at high velocities ($|V_{LSR}| > 100 \text{ km s}^{-1}$) are well characterized down to H I column density levels of $\sim 10^{18} \text{ cm}^{-2}$, but the fundamental properties of most high velocity clouds (HVCs) remain highly uncertain because of limited information about their distances, physical properties, elemental abundances, and dust content (see Wakker & van Woerden 1997 for a review). However, for HVC Complex C and the Magellanic Stream, ultraviolet absorption-line spectroscopy has yielded important information about the elemental composition of the gas and has shed new light on the origins of these HVCs. HVC Complex C lies at a distance $d \gtrsim 10 \text{ kpc}$, has a metallicity of $\sim 0.1\text{--}0.3$ solar, and apparently contains little dust (Wakker et al. 1999; Gibson et al. 2000b; Murphy et al. 2000), which indicates that it is not material ejected into the halo as a consequence of supernovae in the Galactic disk. Rather, it is probably metal-poor infalling gas that may be mixing with circulating Galactic gas at large distances from the Galactic plane. In contrast, H I HVC 287.5+22.5+240 has a metallicity ($S/H = 0.25 \pm 0.07$ solar, Lu et al. 1994a), dust content ($Fe/H \approx 0.033$ solar, Lu et al. 1998), and velocity that suggest it is associated with the Magellanic Stream, an extended ($\sim 100^\circ$) trail of gas pulled out of the Magellanic Clouds during a recent close encounter with the Galaxy (Wannier & Wrixon 1972; Mathewson, Cleary, & Murray 1974).

In this article we report on high-resolution ($\lambda/\Delta\lambda \approx 20,000$) far-ultraviolet (far-UV) absorption-line data obtained for HVC 287.5+22.5+240 with the *Far Ultraviolet Spectroscopic Explorer* (FUSE), a powerful new observatory for studying the molecular, atomic, and ionized gases in HVCs and other interstellar/intergalactic clouds (see Sembach 1999; Oegerle et al. 2000; Sembach et al. 2000b; Shull et al. 2000a). A map of the high velocity H I in the general direction of NGC 3783 is shown in Figure 1. A fortuitous alignment of HVC 287.5+22.5+240 and the nucleus of NGC 3783 ($l = 287.46^\circ$, $b = +22.95^\circ$), a Seyfert 1 galaxy with a bright ultraviolet continuum, makes it possible to study the HVC in absorption below 1200 \AA with FUSE. The HVC has been studied previously in H I 21 cm radio emission (Mathewson et al. 1974; Hulsbosch 1975; Morras & Bajaja 1983; Wakker et al. 1999) and at longer UV wavelengths with the *Hubble Space Telescope* (HST) by Lu et al. (1994a, 1998)⁴. The HVC position and velocity of $+240 \text{ km s}^{-1}$ are consistent with gas arising in the Leading Arm of the Magellanic Stream. The Leading Arm is predicted by N-body simulations tracing the tidal interactions of the Clouds and the Galaxy (Gardiner & Noguchi 1996) and has been identified in H I 21 cm emission (Putman et al. 1998; Putman 2000).

The FUSE spectrum of NGC 3783 contains unique signatures of the absorption within HVC

⁴This HVC is identified as HVC 187 in the Wakker & van Woerden (1991) catalog of high velocity clouds.

287.5+22.5+240, including the first detections of H_2 in the Magellanic Stream. The spectrum also allows for a quantitative estimate of the ionized gas content of the HVC to be made, which is crucial for determining accurate abundances. This is particularly important in light of recent FUSE results showing that many HVCs have a collisionally ionized component seen in O VI absorption. This highly ionized gas probably occurs at either the interfaces or mixing layers between neutral HVC gas and a hot Galactic halo or within cooling regions of hot gas clouds as they are accreted onto the Galaxy (Sembach et al. 2000b).

This paper is organized as follows: Section 2 contains a summary of the FUSE observations and data processing. In §3 we describe the HVC absorption and our measurements of various species. In §4 we consider the atomic and molecular components of the HVC and provide a short description of the intermediate velocity gas along the sight line. In §5 we discuss the FUSE results and their implications for the origin and evolution of HVC 287.5+22.5+240 and the Magellanic Stream.

2. Observations and Data Reduction

The FUSE data for this investigation were obtained on 2 February 2000 and are stored in the FUSE archive at the Multi-Mission Archive at the Space Telescope Science Institute under the identifications P10133001 through P10133013. FUSE contains two microchannel plate detectors and four co-aligned optical channels, with two channels covering shorter wavelengths (SiC; 905–1100 Å) and two channels optimized for longer wavelengths (Al+LiF; 1000–1187 Å). NGC 3783 was centered in the large (LWRS; $30'' \times 30''$) aperture of the LiF1 channel of detector 1 for 13 exposures totaling 37 ksec. (This is the channel used for guiding.) All four channels were reasonably well co-aligned throughout the observation, but the exposure times on the SiC2 and LiF2 channels were limited to 19.5 ksec by the shutdown of detector 2 during exposures 9–13. Most of the FUSE band is covered by at least two channels, except for a few small spectral intervals ($\lambda < 916$ Å, $\lambda > 1182$ Å). We restrict our attention in this article to the data from the LiF1 channel and use the LiF2 data to check for fixed-pattern noise and artifacts. At wavelengths where the LiF channels do not provide coverage because of gaps between the detector segments ($\sim 1082 - 1095$ Å), we use data from the SiC2 channel. A more complete description of the instrument is given by Moos et al. (2000), and the on-orbit performance is discussed by Sahnou et al. (2000).

The raw time-tagged photon event lists for each exposure were run through the standard FUSE calibration pipeline (CALFUSE v1.7.5) available at the Johns Hopkins University as of June 2000. We screened the lists for valid data with the usual constraints imposed for Earth limb avoidance and passage through the South Atlantic Anomaly. We applied corrections for geometric distortions of the spectra on the detectors, spectral motions on the detectors induced by thermal changes, and Doppler shifts caused by orbital motion. Suitable astigmatism and flatfield calibrations were not available at the time of this study. Therefore, we required that any absorption features analyzed be present in the data from at least two channels. Scattered light and detector backgrounds are

negligible at the flux levels of the absorption lines considered in this study. The processed LiF1A data were rebinned to a sampling interval of $\approx 8 \text{ km s}^{-1}$ per pixel since the extracted data are oversampled. The data have a nominal (astigmatic) spectral resolution of $\sim 20 \text{ km s}^{-1}$ (2.5 pixel FWHM) and $S/N = 10$ to 15 per resolution element. The relative wavelength solution is accurate to approximately 6 km s^{-1} (1σ) when averaged over an entire channel, but there are a few wavelengths where the solution may fail by as much as $10\text{--}15 \text{ km s}^{-1}$ over small ($5\text{--}10 \text{ \AA}$) intervals. We set the zero point of the wavelength scale by comparing the low velocity interstellar lines observed in the FUSE bandpass to the longer wavelength S II and Fe II lines observed with the HST by Lu et al. (1998). This zero point also provides a consistent match between the velocities of the low ion absorption line profiles and the H I 21 cm emission along the sight line.

Selected regions of the FUSE spectrum of NGC 3783 are shown in Figure 2. Prominent interstellar Fe II and Ar I lines are labeled above the spectrum. Absorption features due to H_2 in both the low velocity interstellar gas and the HVC (at $+240 \text{ km s}^{-1}$) are indicated with tick marks. The regular spacing of the H_2 lines in the Lyman series (0–0), (3–0), and (4–0) bands makes identification of the HVC features unambiguous. The continuum, emission, and absorption features intrinsic to NGC 3783 in other portions of the FUSE spectrum will be described by Kaiser et al. (2001) and will not be discussed here, other than to note possible blending with the interstellar lines when appropriate.

3. Interstellar Measurements

The NGC 3783 spectrum is complex, with absorption lines in the HVC overlapping absorption features from the intrinsic systems associated with NGC 3783 and the interstellar medium (ISM) of the Milky Way. For cases where the blending is not too severe, we determined continua for the interstellar and HVC lines in the spectrum by fitting low-order (< 5) Legendre polynomials to nearby ($\pm 500 \text{ km s}^{-1}$) regions of the AGN continuum. Equivalent widths for atomic and molecular lines measured in the high velocity gas are listed in Table 1. The equivalent widths and errors were derived following the prescription outlined by Sembach & Savage (1992). Species detected in the HVC include: H_2 , N I, Si II, and Fe II. Additional atomic species (e.g., H I, C II, C III, and O I) are present but are severely blended with other absorption features or fall in wavelength regions of low data quality.

In Table 1 we have included values for the N II $\lambda 1083.99$ line and three lines of H_2 in the Lyman (0–0) vibrational band near 1092 \AA . We measured these lines using the available SiC2 data since they fall in the LiF wavelength gap. The SiC2 data are of lower quality, so these values have larger errors.

A selection of continuum normalized line profiles is shown in Figure 3. The stronger atomic lines reveal absorption at low velocities ($V_{LSR} \sim 0 \text{ km s}^{-1}$), at intermediate velocities ($V_{LSR} \sim +60 \text{ km s}^{-1}$) and at high velocities ($V_{LSR} \sim +240 \text{ km s}^{-1}$). These velocity components correspond to

local gas in the disk of the Galaxy, intermediate velocity gas in the low halo ($z \sim 5$ kpc, assuming corotation with underlying disk gas), and high velocity gas in the HVC. Column densities for all of the atomic lines listed in Table 1 were calculated by direct integration of the apparent optical depth profiles (Savage & Sembach 1991) defined by:

$$N_a = \int N_a(v) dv = \frac{3.768 \times 10^{14}}{f\lambda} \int \tau_a(v) dv \quad (cm^{-2}) \quad (1)$$

where $\tau_a(v)$ is the apparent optical depth of the line (equal to the natural logarithm of the estimated continuum divided by the observed intensity) at velocity v (in $km\,s^{-1}$), f is the oscillator strength of the line, and λ is the wavelength of the line (in \AA). For the lines considered here, $N \approx N_a$ since comparisons of the Fe II $\lambda\lambda 2344.214, 2374.461$ lines observed by the GHRS show that there are no significant unresolved saturated structures within the atomic gas (see Figure 3 in Lu et al. 1998). The GHRS data have a resolution that is better than the FUSE data ($\sim 13\, km\,s^{-1}$ versus $\sim 20\, km\,s^{-1}$), but the HVC lines observed by FUSE are weaker than the longer wavelength Fe II lines (see Figure 3).

4. Results for HVC 287.5+22.5+240

4.1. Atomic Species

Several atomic species are detected in HVC 287.5+22.5+240. Detections free of contamination by other absorption features are available for the lines of N I $\lambda 1134.415$, Si II $\lambda 1020.699$, and Fe II $\lambda 1144.938$. There is a marginal detection of N II derived from the $1083.990\, \text{\AA}$ line, but this detection is of lower quality since it was obtained using SiC2 data. Upper limits can be derived for Fe II $\lambda\lambda 1143.226, 1125.448$; Fe III $\lambda 1122.526$; P II $\lambda 1152.818$; and P III $\lambda 998.000$. An additional upper limit can also be derived for the Ar I $\lambda 1048.220$ line, which occurs on the blue wing of the Lyman (4-0) R(0) line at $1049.367\, \text{\AA}$ (see Figure 2).

The combination of the Fe II and Si II detections with the limits available for other species allows us to check the HVC metallicity and depletion estimates made by Lu et al. (1998). They derived $[S/H] = -0.60 \pm_{0.15}^{0.11}$ and $[Fe/H] = -1.48 \pm 0.07$ assuming $N(H\, I) = 8 \times 10^{19}\, cm^{-2}$, as determined from a comparison of single dish 21 cm emission measurements and an interferometric map of the 21 cm emission with a spatial resolution of $1'$ (Wakker et al. 1999).⁵ The interferometric data reveal a compact concentration of H I in the direction of NGC 3783.

⁵Throughout this work we use the notation: $[X/H] = \log(N(X^i)/N(H^0)) - \log(X/H)_\odot$, where X^i is the dominant ionization stage of element X in neutral gas, and $(X/H)_\odot$ is the solar system meteoritic (or photospheric) abundance ratio of element X to H given by Anders & Grevesse (1989) or Grevesse & Noels (1993) (see Table 2). Since many of the ions dominant in the neutral gas can also be present in ionized regions, all ionization corrections refer to the amount by which $[X/H]$ as defined above needs to be adjusted to account for the fraction of ion X^i produced in

We find that the strengths of the far-UV Fe II lines (see Table 1) are consistent with those of the Fe II $\lambda\lambda 2374.461, 2344.214$ lines observed by Lu et al. (1998). The Fe II column density for the HVC remains unchanged at $\log N(\text{Fe II}) = 13.93 \pm 0.05$. Combining this result with an upper limit of $\log N(\text{Fe III}) < 13.14$ (2σ) yields $N(\text{Fe III})/N(\text{Fe II}) < 0.16$. For a dilute, fully ionized gas with properties similar to those of the warm ionized interstellar medium ionized by O stars ($U = \langle n_\gamma/n_H \rangle \approx 6 \times 10^{-5}$; $n(\text{H}^+)/n(\text{H}) > 0.8$; $n_e \approx 0.08 \text{ cm}^{-3}$), $N(\text{Fe III})/N(\text{Fe II}) \gtrsim 1$ (Sembach et al. 2000a). Therefore, the expected ionized gas contribution to the observed Fe II column is $\lesssim 10 - 15\%$. Unfortunately, it is not possible to estimate the strength of the S III $\lambda 1012.502$ line in the HVC for comparison with the previous S II measurements. The line is blended with strong high velocity H₂ Werner (0–0) Q(3) 1012.680 Å and Lyman (7–0) R(0) 1012.810 Å absorptions and low velocity Lyman (7–0) R(1) 1013.435 Å absorption. Corrections accounting for the amount of singly ionized Si, P, and S arising in H II regions could be somewhat higher than for Fe in the same type of gas but would still be modest. Our Fe III/Fe II result confirms the simple ionization model advanced by Lu et al. (1998) that showed that ionization corrections to the abundances derived for the neutral gas from singly ionized species should be less than 20%.

Higher ionization gas does not contribute significantly to the amount of material in the HVC along the NGC 3783 sight line. Lu et al. (1994) estimated $W_\lambda(\text{C IV } \lambda 1548.195) < 70 \text{ mÅ}$ (2σ) and $W_\lambda(\text{N V } \lambda 1238.821) < 40 \text{ mÅ}$ (2σ), which correspond to $\log N(\text{C IV}) < 13.24$ and $\log N(\text{N V}) < 13.27$. The C IV result implies that the amount of ionized hydrogen associated with highly ionized gas is $\log N(\text{H II}) < 17.3$, or less than 0.2% of the H I column, assuming a metallicity of 0.3 solar and a factor of 2 depletion of carbon onto dust grains. Although O VI absorption is observed toward NGC 3783 at lower velocities ($V_{LSR} < 150 \text{ km s}^{-1}$), it is not possible to quantify the amount of O VI in the HVC since it is confused by redshifted intrinsic H I Ly β absorption⁶ near the O VI $\lambda 1031.926$ line and by Galactic interstellar lines (high velocity C II $\lambda 1036.337$ and H₂ Lyman (5–0) R(1) $\lambda 1037.149$, and low velocity H₂ Lyman (5–0) P(1) $\lambda 1038.157$ and R(2) $\lambda 1038.689$) near the O VI $\lambda 1037.617$ line.

A summary of the abundances for the HVC based upon the HST and FUSE data is given in Table 2. These results are presented graphically in Figure 4. Sulfur and phosphorus, which are elements found primarily in the gas and are not heavily incorporated into dust grains (Jenkins 1978; Savage & Sembach 1996), have abundances of about 0.2 – 0.4 solar in the HVC; they should provide reliable measures of the metallicity of the gas. The limits for N and Ar loosely bracket the S and P values, which is reassuring since N and Ar are found predominantly in neutral (H I) regions. The metallicity of the HVC is identical to the value of $(\text{S}/\text{H}) \sim 0.2\text{--}0.4$ solar found for the

ionized (H^+) gas.

⁶NGC 3783 has a reported redshift of 0.00973 ± 0.00001 ($2919 \pm 3 \text{ km s}^{-1}$) (Theureau et al. 1998). Variable intrinsic absorption has been noted; several prominent absorbers are present at velocities of ~ -560 and $\sim -1420 \text{ km s}^{-1}$ with respect to the systemic velocity of the nuclear emission lines (Crenshaw et al. 1999). Additional highly ionized absorbers within $\sim 600 \text{ km s}^{-1}$ of the systemic velocity have also been seen with the Chandra X-ray Observatory (Kaspi et al. 2000).

Magellanic Stream in the direction of Fairall 9 ($l = 295.07^\circ$, $b = -57.83^\circ$) (Lu, Savage, & Sembach 1994b; Gibson et al. 2000a). Comparing the abundances of S and P with those of Si and Fe shows that these latter two elements are incorporated into dust grains. We find $[\text{Fe}/\text{S}] = -0.88 \pm_{0.17}^{0.12}$ and $[\text{Si}/\text{S}] = -0.21 \pm_{0.21}^{0.14}$. These relative gas-phase abundances are similar to those determined for warm clouds in the Galactic halo (Sembach & Savage 1996) and the Magellanic Bridge (Lehner et al. 2000). The relative levels of Si and Fe depletion are intermediate to the levels derived for gas in the Small Magellanic Cloud (SMC) and the Large Magellanic Cloud (LMC). For the Sk 108 sight line in the SMC, Welty et al. (1997) find $[\text{Zn}/\text{H}]_{\text{SMC}} = -0.64 \pm_{0.17}^{0.13}$, $[\text{Si}/\text{Zn}]_{\text{SMC}} = +0.07 \pm_{0.09}^{0.07}$, and $[\text{Fe}/\text{Zn}]_{\text{SMC}} = -0.57 \pm_{0.09}^{0.07}$. Slightly more severe Si and Fe depletions are observed in the LMC ($[\text{Si}/\text{Zn}]_{\text{LMC}} \approx -0.02$ to -0.18 ; $[\text{Fe}/\text{Zn}]_{\text{LMC}} \approx -0.41$ to -1.18 ; Welty et al. 1999), but the overall metallicity of HVC 287.5+22.5+240 appears to be at least a factor of 2 lower than that of the LMC gas.

4.2. Molecular Hydrogen

H_2 lines arising in the low velocity ISM and the HVC blanket the NGC 3783 spectrum at wavelengths $\lambda < 1120 \text{ \AA}$. Absorption by molecular hydrogen at the velocities of the HVC is most readily apparent in the $J = 1 - 3$ rotational levels in the Lyman series (0–0), (3–0), and (4–0) vibrational bands shown in Figure 2. The $J = 0$ lines in the spectrum are frequently blended with other features, making a determination of $\text{N}(\text{H}_2)$ in the $J = 0$ level particularly difficult. Most of the measurable lines in levels $J = 1 - 3$ have equivalent widths of 50–200 mÅ. No detectable absorption is present in levels $J \geq 4$.

To estimate the column densities of the $J = 0 - 3$ lines, we measured the equivalent widths of all lines free of blending with other features. These values are listed in Table 1. We then constructed a single-component Maxwellian curve of growth and minimized the residuals about the best fit curve for the lines within each level. This resulted in the curve of growth shown in Figure 5. We find a Doppler parameter $b = 12 \pm 2 \text{ km s}^{-1}$ and column densities $\log \text{N}_J(\text{H}_2) = 16.24 \pm 0.20$, 16.64 ± 0.10 , 15.20 ± 0.08 , and 14.80 ± 0.08 for $J = 0, 1, 2$, and 3 , respectively (Table 1). The errors on $\text{N}_J(\text{H}_2)$ are the standard deviations of the data points about the best fit values of $\log(\text{N}f\lambda)$ for the $b = 12 \text{ km s}^{-1}$ single-component curve of growth in Figure 5. The value of $\text{N}_1(\text{H}_2)$ and its error are more uncertain than for the other levels because of the small number of data points available.

The H_2 b -value is smaller than the b -value of 18 km s^{-1} found by fitting the Fe II lines to a single-component curve of growth. We interpret this to mean that the H_2 arises within a more confined region of the HVC than the Fe II. In both cases it is likely that the broadening of the profiles is governed mainly by turbulent motions and substructure within the profiles. As long as the distribution of component widths is not strongly bimodal, a single-component curve of growth approximation and the $\text{N}_a(v)$ analyses used in this work should yield reliable column densities. (See Jenkins 1986 and Savage & Sembach 1991 for discussions of how varying component distributions can affect the column density results.)

We checked the single component curve-of-growth results by fitting instrumentally-smearred Gaussian profiles of varying column density and width to the H_2 lines listed in Table 1. We assumed an instrumental resolution of $\sim 20 \text{ km s}^{-1}$ (FWHM) for all of the lines studied. Values of b smaller than 10 km s^{-1} do not match the data in all rotational levels simultaneously (i.e., not all levels fall on the same curve of growth). Values of b larger than 15 km s^{-1} produce profiles that are broader than the observed profiles.

The total H_2 column density of the HVC in levels $J = 0 - 3$ for $b = 12 \text{ km s}^{-1}$ is $\log N(\text{H}_2) = 16.80 \pm 0.10$. We find $\log N_J(\text{H}_2) \lesssim 14.5$ for levels $J \geq 4$. The fractional abundance of molecular hydrogen in the HVC is $f_{\text{H}_2} = 2N(\text{H}_2)/[N(\text{H I}) + 2N(\text{H}_2)] = 1.6 \times 10^{-3}$. This value⁷ falls in between the values of $f_{\text{H}_2} < 2 \times 10^{-4}$ and $f_{\text{H}_2} > 5 \times 10^{-2}$ found for most diffuse interstellar clouds (Spitzer & Jenkins 1975). In Figure 6 we show an excitation diagram for the first five rotational levels of H_2 in the HVC. The column density of each level divided by the statistical weight of the level is plotted against excitation energy. A Boltzmann distribution described by a single temperature does not adequately describe the distribution of the data points. We find that a temperature, $T_{01} = 133 \pm_{21}^{37} \text{ K}$ describes the relative populations of the $J = 0$ and $J = 1$ levels, while a higher temperature, $T_{23} = 241 \pm_{17}^{20} \text{ K}$, is needed to describe the relative populations of the $J = 2$ and $J = 3$ levels. In both cases, the temperatures were derived from the usual ratios of column densities and statistical weights (Spitzer et al. 1974) given by

$$T_{ij} = \frac{E_j - E_i}{k \ln[(g_j/g_i)(N_i/N_j)]} \quad (2)$$

The derived value of $T_{01} \approx 133 \text{ K}$ is higher than the value of $\langle T_{01} \rangle \sim 80 \text{ K}$ derived for sight lines in the Galactic disk (Spitzer & Cochran 1973; Savage et al. 1977), but is similar to the values found for diffuse interstellar clouds along high latitude sight lines toward quasars and AGNs (Shull et al. 2000b). An elevated rotational excitation temperature derived for levels $J \geq 2$ compared to the temperature derived from levels $J = 0 - 1$ is common in studies of H_2 absorption and may be due to a variety of processes, including photon pumping of the higher J levels, shocks, and formation of H_2 on dust grains (see Shull & Beckwith 1982 and references therein). This last mechanism, “formation pumping”, involves the excitation of rotational and vibrational states produced when newly-formed molecules are ejected from grain surfaces. The 4.48 eV of H_2 latent heat of formation can appear as kinetic energy, ro-vibrational (v, J) excitation, or phonon (heat) energy in the grain, all in highly uncertain proportions. If even 10–20% of this energy appears as H_2 excitation, significant excitation of the upper- J states in $v = 0$ is possible. Radiative cascade from the initial formation entry, through the quadrupole lines from low vibrational states, removes a good deal of the memory of the initial excitation. The resulting rotational excitation is similar to that of radiative excitation.

⁷This standard definition of f_{H_2} does not account for $N(\text{H}^+)$, which is generally small in comparison to the amount of neutral gas present in the interstellar clouds considered here.

4.3. The Intermediate Velocity Cloud Near +62 km s⁻¹

H₂ absorption is convincingly detected only near 0 and +240 km s⁻¹ in the direction of NGC 3783 (see Figure 3). The intermediate velocity gas seen near +62 km s⁻¹ in H I 21 cm emission and in the Si II and Fe II absorption lines shown in the left panel of Figure 3 is free of H₂ absorption down to a level of $\log N(\text{H}_2) \lesssim 15.6$. Table 3 contains upper limits on $N_J(\text{H}_2)$ derived from several transitions for which the 30–75 km s⁻¹ velocity range does not contain absorption due to other lines. A more stringent limit of $\log N(\text{H}_2) \lesssim 15.0$ can be derived by assuming $T_{01} > 100$ K and using the observed limit of $\log N_1(\text{H}_2) < 14.74$. For this intermediate velocity cloud (IVC), Wakker et al. (2000) find $\log N(\text{H I}) \approx 20.0$ from 21 cm data obtained with a 15' beam at Parkes. Using this value, we derive $f_{\text{H}_2} \lesssim 2 \times 10^{-5}$ if $T > 100$ K.

Direct integration of the S II and Fe II apparent column density profiles obtained with the GHRS and FUSE over the velocity range +30 to +130 km s⁻¹ yields $\log N(\text{S II}) = 15.01 \pm 0.05$ and $\log N(\text{Fe II}) = 14.74 \pm 0.03$. The resulting gas-phase abundances are $[\text{S}/\text{H}] = -0.27 \pm 0.05$ (as found by Lu et al. (1994a)) and $[\text{Fe}/\text{S}] = -0.26 \pm 0.06$, which implies that most of the Fe is in the gas. Some of the intermediate velocity gas could be ionized; the amount of Fe III over the same velocity range is $\log N(\text{Fe III}) < 14.22$, which implies that most (> 70%) of the Fe II is in the neutral gas. The Fe depletion is very small compared to values expected for clouds in the Milky Way disk, where $[\text{Fe}/\text{S}] \sim -1.2$ to -2.5 dex (Savage & Sembach 1996).

The scarcity of H₂ and dust grains in the intermediate velocity gas compares favorably to recent H₂ measurements for other IVCs located in the low halo. In the direction of PG 0804+761, Richter et al. (2000) find $[\text{Fe}/\text{H}] = -0.75 \pm 0.05$ and $f_{\text{H}_2} = 2.97 \times 10^{-5}$ in the -55 km s⁻¹ gas of the Low Latitude Intermediate Velocity Arch ($z \approx 0.6$ – 1.2 kpc). Toward HD 93521, Fitzpatrick & Spitzer (1993) find $[\text{Fe}/\text{H}] = -0.61 \pm 0.11$ in the warm halo clouds near -60 km s⁻¹ ($z \sim 0.3$ – 1.5 kpc), and the H₂ measurements of Gringel et al. (2000) yield $f_{\text{H}_2} = 2.0 \times 10^{-5}$ assuming $\log N(\text{H I}) = 19.61$ for the same clouds (components 1–5 in Table 2 of Spitzer & Fitzpatrick 1993). Thus, the observed velocity, molecular fraction, and dust content of the IVC toward NGC 3783 are consistent with the idea that the IVC is part of a co-rotating, off-plane ($z \approx 5$ kpc) extension of an outer spiral arm as suggested by Lu et al. (1994a).

5. Discussion

5.1. The Origin and Properties of HVC 287.5+22.5+240

The elemental abundances, kinematics, and position of HVC 287.5+22.5+240 all indicate that the HVC is part of the Leading Arm of the Magellanic Stream. The tidal plus weak drag model proposed by Gardiner (1999) shows that the material in the Leading Arm was stripped primarily from the disk of the SMC and is located a distance of about 50–75 kpc from the Sun. This feature is observed in sensitive H I 21 cm maps of the Magellanic Stream (Putman et al. 1998,

2000). A detailed study of the high velocity H I 21 cm emission in the direction of NGC 3783 at different angular resolutions by Wakker et al. (1999) reveals that discrete structures exist on scales down to $1'$ ($= 14.5$ pc at a distance $D = 50$ kpc). They estimate that the HVC is part of an ensemble of small gas clouds with internal thermal pressures, $P/k \sim 18,000 D_{kpc}^{-1} \text{ K cm}^{-3}$, implying $P/k = 1.1 n_H T \sim 360 \text{ K cm}^{-3}$ for an assumed distance of 50 kpc.

The number of high velocity clouds for which both gas-phase abundances and molecular content are available is very limited. The two highest quality measurements to date are for HVC 287.5+22.5+240 (the subject of this paper) and Complex C. For HVC 287.5+22.5+240, we find $N(\text{H}_2) = 6.3 \times 10^{16} \text{ cm}^{-2}$ and $f_{\text{H}_2} = 1.6 \times 10^{-3}$. We infer the presence of dust from the relative abundances of Si, S, and Fe (§ 4.1). For Complex C in the direction of Mrk 876 ($l = 98.27^\circ, b = +40.38^\circ$), Murphy et al. (2000) find $N(\text{H}_2) < 2 \times 10^{14} \text{ cm}^{-2}$ and $f_{\text{H}_2} < 1.7 \times 10^{-5}$. Combined with the abundance information available for Fe from FUSE (Murphy et al. 2000) and sulfur from HST (Wakker et al. 1999; Gibson et al. 2000b), it appears that Complex C has a low metallicity ($\sim 0.1 - 0.3$ solar) and essentially no depletion of Fe onto dust grains. Thus, these two cases imply that dust and H_2 are related in HVCs – low values of f_{H_2} and mild depletions appear to go together.

High velocity H_2 has also been reported for HVCs in the direction of the LMC, although the detections are not as secure as the detection for HVC 287.5+22.5+240. Using the echelle spectrograph on the *Orbiting and Retrieivable Far and Extreme Ultraviolet Spectrometers* (ORFEUS), Richter et al. (1999) found $N(\text{H}_2) = (2.2 - 3.6) \times 10^{15} \text{ cm}^{-2}$ and $f_{\text{H}_2} = (3.6 - 6.0) \times 10^{-4}$ in the $+120 \text{ km s}^{-1}$ HVC toward the LMC star HD 269546 ($l = 279.32^\circ, b = -32.77^\circ$)⁸. Their analysis of *International Ultraviolet Explorer* (IUE) Fe II data indicated that (Fe/H) in the cloud is roughly half the solar value. Several higher quality observations of other LMC stars by FUSE also reveal H_2 absorption and will allow a more thorough investigation of the composition and molecular fraction of the high velocity gas in front of the LMC (Richter et al. 2001).

5.2. Where did the H_2 Originate?

The presence of molecular gas in HVC 287.5+22.5+240 requires that either the H_2 formed in situ or that the H_2 was originally formed in the SMC and survived the tidal stripping that created the Leading Arm. For the six LMC and one SMC sight lines for which Magellanic Cloud H_2 was observed with ORFEUS or the *Hopkins Ultraviolet Telescope* (HUT), four have values of $f_{\text{H}_2} < 1 \times 10^{-4}$, one has a value of 6.6×10^{-3} , and two have values $> 3.8 \times 10^{-2}$ (see Richter 2000 and references therein). FUSE observations of a much larger sample of stars (~ 40) demonstrate that H_2 is often present in the Clouds; preliminary results for 10 stars in both the LMC and SMC (Tumlinson et al. 2001) yield $\langle f_{\text{H}_2} \rangle \approx 1.5 \times 10^{-2}$ in the LMC and $\langle f_{\text{H}_2} \rangle \approx 9.0 \times 10^{-3}$ in the SMC,

⁸As this paper was being refereed, HD 269546 (Sk-6882) was observed with FUSE. The FUSE spectra indicate that the H_2 absorption is weaker than deduced from the ORFEUS data (P. Richter, private communication). This suggests that f_{H_2} for the $+120 \text{ km s}^{-1}$ gas in the LMC direction may be less than the value stated above.

with a range of values encompassing both the low and high f_{H_2} branches. However, few points fall in the “transition” region between low and high f_{H_2} . In this respect, the Magellanic Cloud molecular hydrogen fractions resemble those found for Milky Way disk and halo gas (Savage et al. 1977; Shull et al. 2000b). If the H_2 in HVC 287.5+22.5+240 is remnant material stripped from the SMC, it likely originated in a region having a higher value of f_{H_2} than the presently observed value of 1.6×10^{-3} .

The formation and destruction of H_2 are influenced by many competing factors. These include the quantity and type of dust grains, the gas density, the amount of self-shielding by the H_2 , the intensity of the far-ultraviolet radiation field, the presence of hot gas, and the effects of shocks. At the column density levels observed, it is unlikely that the H_2 in the HVC is thermalized, and in a dynamic environment such as the Magellanic Stream the competing production and destruction effects may not be equilibrated. Thus, it is difficult to quantify the net H_2 production rate. However, it is still useful to briefly consider what some of the competing effects may be.

Dust grains serve as catalysts for the formation of H_2 (Hollenbach, Werner, & Salpeter 1971; Spitzer & Jenkins 1975) and also act as a shielding agent against ultraviolet photons capable of dissociating the molecules. The formation of H_2 proceeds most readily for high grain surface area and cold gas and grain temperatures. The heavy element abundance pattern in the HVC is similar to that in warm ($T \sim 10^3$ K) clouds located in the Galactic halo, which suggests that the grains have been stripped of their outer mantles and consist mainly of their residual (oxide) cores (Sembach & Savage 1996). Thus, much of the grain surface has probably been modified and may be less conducive to H_2 formation than the surfaces of grains found in cold molecular clouds in the Galactic disk.

The ultraviolet radiation field at the location of the Leading Arm is probably less intense than for typical interstellar environments within either the Galaxy or the SMC. The exact details of the radiation field and heating of the gas depend upon the transfer of photons out of the Galaxy and the Magellanic Clouds (see Wolfire et al. 1995; Bland-Hawthorn & Maloney 1999). The rotational excitation temperatures derived for HVC 287.5+22.5+240 are consistent with modest photon pumping of the $J = 2$ and 3 levels but are not indicative of very high levels of excitation like those found for clouds near hot stars (no higher rotational level lines are seen). To date, no early-type stars have been found in the Magellanic Stream. In the Galaxy, much higher excitation temperatures ($T_{ex} > 500$ K) are often found for H_2 in the vicinity of hot stars, and similarly high values have been observed for interstellar gas in the Magellanic Clouds (e.g., Friedman et al. 2000; Mallouris et al. 2001; Tumlinson et al. 2001).

The absorbing clouds have 21 cm emission structure on the scale of $\sim 1' - 10'$ (Putman & Gibson 1999; Wakker et al. 1999), which corresponds to sizes of $\sim 1 - 100$ pc at the estimated 50 kpc distance of the HVC. The corresponding temperature range is $\sim 100 - 1000$ K, if the pressure model of §5.1 is correct. Directly along the NGC 3783 sight line, the H I 21 cm emission has FWHM ≈ 22 km s $^{-1}$ (see Figure 2 in Lu et al. 1998). For a line broadened solely by thermal gas motions,

this corresponds to $T = 21.7(FWHM)^2 \approx 10^4$ K. However, this is an upper limit since the line may also be broadened significantly by turbulence and sub-component structure. This appears to be the case since the lines of species heavier than H I (e.g., Si II, Fe II) are also broad and have effective b-values much larger than those expected for thermal motions alone (see Figure 3 and § 4).

If we adopt a gas pressure, $P/k = 360 \text{ cm}^{-3} \text{ K}$, and assume $T = (100 \text{ K})T_{100}$ with $\text{He}/\text{H} = 0.1$, the hydrogen density is $n_H = (3.3 \text{ cm}^{-3})(T_{100})^{-1}$, from which we estimate a characteristic cloud dimension of $L = N(\text{H I})/n_H = (8 \text{ pc})(T_{100})$. The observations are therefore consistent with $0.3 < n_H < 3 \text{ cm}^{-3}$ for $100 < T < 1000 \text{ K}$. This range of densities is in the low- n_H limit for models of H_2 radiative excitation and collisional de-excitation. Preliminary estimates based on fitting the populations of rotational levels $J = 2$ and $J = 3$ suggest that the H_2 absorption rate in the Lyman and Werner bands (1000 \AA) is $\beta_{\text{uv}} < 5 \times 10^{-11} \text{ s}^{-1}$, or < 0.1 times the average value, $\beta_0 = 5 \times 10^{-10} \text{ s}^{-1}$ in the solar neighborhood (Jura 1974).

The other general statement that can be made concerning the origin of H_2 in this HVC is the characteristic formation time. The H_2 formation rate depends on the collision rate between H I atoms and grains, the probability that H I atoms are adsorbed on the grain surface (“sticking probability”), the mobility and lifetime of the atoms on the surface, and the probability that a molecule is ejected after formation. The volume formation rate of H_2 on grain surfaces (Hollenbach & Salpeter 1971; Shull & Beckwith 1982) is written as Rn_H , where $R \approx (1 - 3) \times 10^{-17} \text{ cm}^3 \text{ s}^{-1}$ in the local ISM. Molecule formation proceeds rapidly for grains with surface temperatures less than a critical value, $T_{\text{cr}} \approx 20 - 100 \text{ K}$; H_2 formation may also be suppressed when $T_{\text{HI}} \gg 100 \text{ K}$. For the range of physical conditions for this HVC, we estimate the H_2 formation time to be,

$$t_{\text{form}} \approx [Rn_{\text{HI}}]^{-1} \approx 1 \times 10^8 \text{ yr} \quad (3)$$

for $R \approx 10^{-17} \text{ cm}^3 \text{ s}^{-1}$ and $n_H = n_{\text{HI}} \approx 3 \text{ cm}^{-3}$. Although this time is a significant fraction of the ($\sim 1 \text{ Gyr}$) orbital period of the Magellanic Stream, new H_2 could form up to the observed fraction, $f_{\text{H}_2} \approx 10^{-3}$, on the surfaces of dust grains that survived the process of tidal stripping. More likely, much of the observed H_2 survived stripping and has resisted photodestruction by the high-latitude ultraviolet radiation field because of self-shielding in the dissociating Lyman bands. Self-shielding becomes important and reduces the destruction rate ($\langle k \rangle \beta_{\text{uv}}$) by a substantial factor once $N(\text{H}_2) \gg 10^{14} \text{ cm}^{-2}$ (optical depth unity in the Lyman band).

5.3. Relevance to QSO Absorption Lines

Absorption line spectroscopy of the Lyman and Werner bands of H_2 provides the most sensitive means available for assessing the molecular content of cold gas in the Universe. To date, detections of H_2 absorption outside the Milky Way have been limited to the Magellanic Clouds (see Richter 2000; Shull et al. 2000b; Mallouris et al. 2001; Tumlinson et al. 2001), a few high redshift ($z \gtrsim 2$) quasar absorption line systems (Levshakov & Varshalovich 1985; Ge & Bechtold 1997; Levshakov et al. 2000), and now HVC 287+22.5+240. Although a few low column density quasar absorption

line systems have modest values of f_{H_2} , most have very little molecular gas and do not appear to sustain a large quantity of molecules due to the intense radiation field impinging on the clouds (see Black, Chaffe, & Foltz 1987; Levshakov et al. 2000). These systems also contain little dust. HVCs represent the best low-redshift analogs to the QSO absorption line systems with $17 \lesssim \log(\text{H I}) \lesssim 19$. Therefore, a better understanding of the processes that affect the elemental abundances, molecular content, and dust composition of HVCs could provide important insights into similar quantities derived for the quasar absorption line systems. This is especially important for HVCs that originate either from tidal interactions (as appears to be the case for HVC 287.5+22.5+240) or are part of a larger ensemble of extragalactic clouds in the Local Group that may be interacting with the Milky Way (see, e.g., Blitz et al. 1999; Sembach et al. 1999, 2000b). If such dust-bearing clouds commonly exist around other galaxies, particularly those at high redshift, the dust could produce intragroup reddening that might affect studies of objects in those distant galaxies (e.g., the dimming of very distant supernovae used to study the expansion of the Universe).

We thank the FUSE Science and Operations Teams for their dedicated efforts to make the observations described in this paper possible. We also thank Mary Putman and Brad Gibson for providing a preliminary electronic version of Figure 1, Philipp Richter and Daniel Welty for useful comments on the manuscript, and Matthew Browning for assistance with the calculation of β_{uv} . This work is based on data obtained for the FUSE Science Team by the NASA-CNES-CSA FUSE mission operated by the Johns Hopkins University. Financial support has been provided by NASA contract NAS5-32985. KRS and JCH acknowledge partial support from NASA Long Term Space Astrophysics grant NAG5-3485. JMS acknowledges support from NASA LTSA grant NAG5-7262.

REFERENCES

- Abgrall, H., Roueff, E., Launay, F., Roncin, J.Y., & Subtil, J.L. 1993a, A&AS, 101, 273
- Abgrall, H., Roueff, E., Launay, F., Roncin, J.Y., & Subtil, J.L. 1993b, A&AS, 101, 323
- Anders, E. & Grevesse, N. 1989, *Geochim. Cosmochim. Acta*, 53, 197
- Black, J.H., Chaffee, F.H., & Foltz, C.B. 1987, *ApJ*, 317, 442
- Blitz, L., Spergel, D., Teuben, P., Hartmann, D., & Burton, W.B. 1999, *ApJ*, 514, 818
- Crenshaw, D.M., Kraemer, S.B., Boggess, A., Maran, S.P., Mushotsky, R.F., & Wu, C.-C. 1999, *ApJ*, 516, 750
- Federman, S.R., Glassgold, A.E., & Kwan, J. 1979, *ApJ*, 227, 466
- Friedman, S.D., et al. 2000, *ApJ*, 538, L39
- Gardiner, L.T. 1999, in *The Stromlo Workshop on High Velocity Clouds*, ASP Conf. Series 166, eds. B.K. Gibson & M.E. Putman, (San Francisco: ASP), 292
- Gardiner, L.T. & Noguchi, M. 1996, *MNRAS*, 278, 191
- Ge, J. & Bechtold, J. 1997, *ApJ*, 477, L73
- Gibson, B.K., Giroux, M.L., Penton, S.L., Putman, M.E., Stocke, J.T., & Shull, J.M. 2000a, *AJ*, vol 120 (astro-ph/0007078)
- Gibson, B.K., Giroux, M.L., Penton, S.L., Stocke, J.T., & Shull, J.M. 2000b, *AJ*, submitted
- Grevesse, N. & Noels, A. 1993, In *Origin and Evolution of the Elements*, eds. N. Prantzos, E. Vangioni-Flam, & M. Cassé, (Cambridge: Cambridge Univ. Press), 15
- Gringel, W., Barnstedt, J., de Boer, K.S., Grewing, M., Kappelman, N., & Richter, P. 2000, *A&A*, 358, L37
- Hollenbach, D. J. & Salpeter, E. E. 1971, *ApJ*, 163, 155
- Hollenbach, D. J., Werner, M.W., & Salpeter, E. E. 1971, *ApJ*, 163, 165
- Howk, J.C. Sembach, K.R., Roth, K.C., & Kruk, J.W. 2000, *ApJ*, in press (astro-ph/0007236)
- Hulsbosch, A.N.M. 1975, *A&A*, 40, 1
- Jenkins, E.B. 1986, *ApJ*, 304, 739
- Jenkins, E.B. 1987, in *Interstellar Processes*, eds. D.J. Hollenbach & H.A. Thronson, (Dordrecht: Reidel), 533
- Jura, M. 1974, *ApJ*, 191, 375
- Kaiser, M.B., et al. 2001, in preparation
- Kaspi, S., Brandt, W.N., Netzer, H., Sambruna, R., Chartas, G., Garmire, G.P., & Nousek, J.A. 2000, *ApJ*, in press (astro-ph/0004050)
- Lehner, N., Sembach, K.R., Dufton, P.L., Rolleston, W.R.J., & Keenan, F.P. 2000, *ApJ*, in press

- Levshakov, S.A., Molaro, P. Centurión, M., D’Odorico, S., Bonifacio, P., & Vladilo, G. 2000, A&A, in press (astro-ph/0007472)
- Levshakov, S.A., & Varshalovich, D.A. 1985, MNRAS, 212, 517
- Lu, L., Savage, B.D., & Sembach, K.R. 1994a, ApJ, 426, 563
- Lu, L., Savage, B.D., & Sembach, K.R. 1994b, ApJ, 437, L119
- Lu, L., Savage, B.D., Sembach, K.R., Wakker, B.P., Sargent, W.L.W., & Oosterloo, T.A. 1998, AJ, 115, 162
- Mallouris, C.M., et al. 2001, in preparation
- Mathewson, D.S., Cleary, M.N., & Murray, J.D. 1974, ApJ, 190, 291
- Moos, H.W., et al. 2000, ApJ, 538, L1
- Morras, R. & Bajaja, E. 1983, A&AS, 51, 131
- Morton, D.C. 2001, in preparation
- Murphy, E.M., et al. 2000, ApJ, 538, L35
- Oegerle, W.R., et al. 2000, ApJ, 538, L23
- Putman, M.E. 2000, PASA, 17, 1
- Putman, M.E. & Gibson, B.K. 1999, PASA, 16, 70
- Putman, M.E., et al. 1998, Nature, 394, 752
- Richter, P. 2000, A&A, 359, 1111
- Richter, P. de Boer, K.S., Widmann, H., Kappelman, N., Gringel, W., Grewing, M., & Barnstedt, J. 1999, Nature, 402, 386
- Richter, P., Savage, B.D., Wakker, B.P., Sembach, K.R., & Kalberla, P.M.W. 2000, ApJ, submitted
- Richter, P., Sembach, K.R., Howk, J.C., & Savage, B.D. 2001, in prep
- Russell, S.C. & Dopita, M.A. 1992, ApJ, 384, 508
- Sahnow, D.S., et al. 2000, ApJ, 538, L7
- Savage, B.D., Bohlin, R.C., Drake, J.F., & Budich, W. 1977, ApJ, 216, 291
- Savage, B.D. & Sembach, K.R. 1991, ApJ, 379, 245
- Savage, B.D. & Sembach, K.R. 1996, ARA&A, 34, 279
- Sembach, K.R. 1999, in *The Stromlo Workshop on High Velocity Clouds*, ASP Conf. Series 166, eds. B.K. Gibson & M.E. Putman, (San Francisco: ASP), 243
- Sembach, K.R., Howk, J.C., Ryans, R.S.I., & Keenan, F.P. 2000a, ApJ, 528, 310
- Sembach, K.R., & Savage, B.D. 1992, ApJS, 83, 147
- Sembach, K.R., & Savage, B.D. 1996, ApJ, 457, 211

- Sembach, K.R., Savage, B.D., Lu, L., & Murphy, E.M. 1999, *ApJ*, 515, 108
- Sembach, K.R., et al. 2000b, *ApJ*, 538, L31
- Shull, J.M. & Beckwith, S. 1982, *ARA&A*, 20, 163
- Shull, J.M., et al. 2000a, *ApJ*, 538, L13
- Shull, J.M., et al. 2000b, *ApJ*, 538, L73
- Spitzer, L. & Cochran, W.D. 1973, *ApJ*, 186, L23
- Spitzer, L., Cochran, W.D., & Hirshfeld, A. 1974, *ApJS*, 28, 373
- Spitzer, L. & Fitzpatrick, E.L. 1993, *ApJ*, 409, 299
- Spitzer, L. & Jenkins, E.B. 1975, *ARA&A*, 13, 133
- Theureau, G., Bottinelli, L., Coudreau-Durand, N., Gouguenheim, L., Hallet, N., Loulergue, M., Paturel, G., & Teerikorpi, P. 1998, *A&AS*, 130, 333
- Tumlinson, J., Shull, J.M., et al. 2001, in prep
- van Dishoeck, E.F. & Black, J.H. 1986, *ApJS*, 62, 109
- Wakker, B.P., Howk, J.C., Savage, B.D., van Woerden, H., Tufte, S.L., Schwarz, U.J., Benjamin, R., Reynolds, R.J., Peletier, R.F., & Kalberla, P.M.W. 1999, *Nature*, 402, 388
- Wakker, B.P., Kalberla, P.M.W., van Woerden, H., de Boer, K.S., & Putman, M.E. 2000, *ApJS*, submitted
- Wakker, B.P., Murphy, E.M., van Woerden, H., & Dame, T.M. 1997, *ApJ*, 488, 216
- Wakker, B.P., Savage, B.D., Oosterloo, T.A., & Putman, M.E. 1999, in *The Stromlo Workshop on High Velocity Clouds*, ASP Conf. Series 166, eds. B.K. Gibson & M.E. Putman, (San Francisco: ASP), 302
- Wakker, B.P. & van Woerden, H. 1991, *A&A*, 250, 509
- Wannier, P. & Wrixon, G.T. 1972, *ApJ*, 173, L119
- Welty, D.E., Lauroesch, J.T., Blades, J.C., Hobbs, L.M., & York, D.G. 1997, *ApJ*, 489, 672
- Welty, D.E., Frisch, P.C., Sonneborn, G., & York, D.G. 1999, *ApJ*, 512, 636
- Wolfire, M.G., Hollenbach, D., McKee, C.F., Tielens, A.G.G.M., & Bakes, E.L.O. 1995, *ApJ*, 443, 152

Table 1. HVC Atomic and Molecular Absorption Lines

Atom/Ion	Wavelength ^a (Å)	f^b	W_λ^c (mÅ)	$\log N^d$ (cm ⁻²)
H I	21 cm	19.90 ± 0.05^e
N I	1134.980	4.35×10^{-2}	84 ± 18	> 14.52
N II	1083.990	1.03×10^{-1}	$99 \pm 42^{f,g}$	$13.97 \pm_{0.24}^{0.15f,g}$
P II	1152.818	2.45×10^{-1}	< 32	< 13.05
P III	998.000	1.12×10^{-1}	< 40	< 13.61
Si II	1020.699	1.64×10^{-2}	56 ± 14	$14.64 \pm_{0.13}^{0.10}$
Ar I	1048.220	2.44×10^{-1}	< 85	$< 14.25^h$
Fe II	1144.938	1.06×10^{-1}	78 ± 17	$13.90 \pm_{0.10}^{0.08}$
	1143.226	1.77×10^{-2}	< 26	< 14.09
	1125.448	1.56×10^{-2}	< 24	< 14.16
Fe III	1122.526	1.62×10^{-2}	< 24	< 13.14
H ₂ ($J = 0$)				
0–0 R(0)	1108.127	1.66×10^{-3}	117 ± 15	16.24 ± 0.20
1–0 R(0)	1092.195	5.90×10^{-3}	85 ± 31^f	...
2–0 R(0)	1077.140	1.15×10^{-2}	$< 360^i$...
H ₂ ($J = 1$)				
0–0 R(1)	1108.633	1.08×10^{-3}	113 ± 15	16.64 ± 0.10
0–0 P(1)	1110.063	5.73×10^{-4}	$< 120^j$	
1–0 R(1)	1092.732	3.88×10^{-3}	159 ± 32^f	...
1–0 P(1)	1094.052	1.97×10^{-3}	112 ± 34^f	...

Table 1—Continued

Atom/Ion	Wavelength ^a (Å)	f^b	W_λ^c (mÅ)	$\log N^d$ (cm ⁻²)
2–0 P(1)	1078.923	3.90×10^{-3}	165 ± 15	...
2–0 R(1)	1077.697	7.84×10^{-3}	201 ± 20	...
3–0 P(1)	1064.606	5.66×10^{-3}	188 ± 14	...
4–0 P(1)	1051.031	7.73×10^{-3}	170 ± 15	...
H ₂ ($J = 2$)				
0–0 Q(2) ^k	1010.938	2.45×10^{-2}	106 ± 15	15.20 ± 0.08
2–0 R(2)	1079.226	6.85×10^{-3}	81 ± 14	...
3–0 R(2)	1064.994	1.07×10^{-2}	93 ± 10	...
3–0 P(2)	1066.899	7.07×10^{-3}	80 ± 12	...
4–0 R(2)	1051.498	1.39×10^{-2}	99 ± 11	...
4–0 P(2)	1053.283	8.98×10^{-3}	93 ± 10	...
7–0 R(2)	1014.977	1.90×10^{-2}	75 ± 13	...
8–0 R(2)	1003.984	1.67×10^{-3}	98 ± 22	...
H ₂ ($J = 3$)				
0–0 P(3)	1115.895	7.73×10^{-4}	< 24	14.80 ± 0.08
1–0 R(3)	1096.725	3.01×10^{-3}	< 30	...
1–0 P(3)	1099.786	2.46×10^{-3}	< 30	...
3–0 R(3)	1067.474	1.01×10^{-2}	58 ± 10	...
3–0 P(3)	1070.138	7.48×10^{-3}	51 ± 10	...
4–0 R(3)	1053.977	1.33×10^{-2}	54 ± 10	...
4–0 P(3)	1056.473	9.56×10^{-3}	$< 120^j$...
7–0 R(3)	1017.423	1.84×10^{-2}	60 ± 10	...
6–0 R(3)	1028.983	1.73×10^{-2}	57 ± 10	...
7–0 P(3)	1019.502	1.05×10^{-2}	45 ± 10	...
8–0 R(3)	1006.413	1.58×10^{-2}	52 ± 17	...
H ₂ ($J = 4$)				

Table 1—Continued

Atom/Ion	Wavelength ^a (Å)	f^b	W_λ^c (mÅ)	$\log N^d$ (cm ⁻²)
3–0 R(4)	1070.899	9.67×10^{-3}	< 36	< 14.6
3–0 P(4)	1074.314	7.81×10^{-3}	< 28	< 14.5
4–0 R(4)	1057.376	1.29×10^{-2}	< 30	< 14.4
4–0 P(4)	1060.580	9.84×10^{-3}	< 28	< 14.5

^aVacuum atomic wavelength from Morton (2001) or molecular wavelength from Abgrall et al. (1993a,b). All molecular lines are Lyman series transitions, except for the Werner band 0–0 Q(2) transition at 1010.939 Å.

^bAtomic f -value from Morton (2001) except for the Fe II lines, which are from Howk et al. (2000). H₂ f -values were calculated from the emission probabilities given by Abgrall et al. (1993a,b).

^cEquivalent width. Errors are 1σ estimates that account for continuum placement uncertainties and statistical noise. Limits are 2σ estimates.

^dAdopted column density. For the atomic lines, the results of direct integrations of the apparent column density profiles are listed. For H₂, the column densities of the rotational levels are given assuming a single component Doppler-broadened curve-of-growth with $b = 12 \text{ km s}^{-1}$. Limits are 2σ estimates.

^eH I column density from Lu et al. (1998). This value is based on an interferometric map with an angular resolution of $1'$.

^fValue measured using lower quality SiC2 data because the line falls in the wavelength gap between LiF1A and LiF1B.

^gThis line may contain a small amount of N II* $\lambda 1084.580$ associated with the IVC at $+62 \text{ km s}^{-1}$. The velocity difference between the HVC and this IVC absorption is $\sim 15 \text{ km s}^{-1}$. Thus, this tentative detection of N(N II) in the HVC should probably be considered an upper limit.

^hColumn density limit assuming the equivalent width limit listed and a single component curve-of-growth having $b = 18 \text{ km s}^{-1}$.

ⁱLine appears stronger than expected due to unknown source of blending.

^jUpper limit due to blending with other H₂ lines.

^kWerner series line.

Table 2. HVC Abundances

Element	$(X/H)_{\odot}^a$	$[X/H]^b$
N	8.55 ± 0.05	> -1.93
Si	7.55 ± 0.02	$-0.81 \pm_{0.12}^{0.09}$
P	5.57 ± 0.04	< -0.42
S	7.27 ± 0.05	$-0.60 \pm_{0.15}^{0.11c}$
Ar	6.56 ± 0.10	< -0.21
Fe	7.51 ± 0.01	-1.48 ± 0.07^d

^aSolar System abundance on a logarithmic scale where the abundance of H is 12. Meteoritic values for Si, P, S, Ar, and Fe are from Anders & Grevesse (1989). The value for N is a solar photospheric value from Grevesse & Noels (1993).

^b $[X/H] = \log N(X^i)/N(H^0) - \log (X/H)_{\odot}$, where $X^i = N \text{ I, Si II, P II, S II, or Fe II}$. Errors in this quantity reflect measurement errors only and do not include errors on $(X/H)_{\odot}$. Ionization corrections for the singly ionized species are less than 20% (i.e., < 0.1 dex).

^cValue from Lu et al. (1998).

^dValue from Lu et al. (1998). Using the value of $N(\text{Fe II}) = 13.90$ in Table 1 for the $\lambda 1144.94$ line, we find $[\text{Fe}/H] = -1.51 \pm_{0.12}^{0.09}$, which is consistent with the higher precision Lu et al. result.

Table 3. Limits on H₂ in the +62 km s^{−1} IVC

H ₂ Line	λ (Å)	f	W_λ ^a (mÅ)	log N _J ^b (cm ^{−2})
0–0 R(0)	1108.127	1.66×10^{-3}	< 49	< 15.44 ^c
4–0 P(1)	1051.031	7.73×10^{-3}	< 42	< 14.74
0–0 Q(2)	1010.938	2.45×10^{-2}	< 41	< 14.27
6–0 R(3)	1028.983	1.73×10^{-2}	< 34	< 14.32
4–0 R(4)	1057.376	1.29×10^{-2}	< 24	< 14.27

^aEquivalent width limit (2σ) between +30 and +75 km s^{−1}.

^bColumn density limit (2σ) assuming a linear curve of growth.

^cA more stringent limit of log N₀(H₂) \lesssim 14.5 can be derived by requiring $T_{01} = 100K$. With such a requirement, log N(H₂) \lesssim 15.0.

Fig. 1.— An H I Parkes All-Sky Survey (HIPASS) map of the high velocity (+170 to +400 km s^{-1}) gas in the general direction of NGC 3783 (Putman & Gibson 1999). The data have an angular resolution of approximately $15.5'$. NGC 3783, marked by a white star symbol, lies behind a large complex of gas believed to be the Leading Arm of the Magellanic Stream. A higher resolution map of this cloud can be found in Wakker et al. (1999).

Fig. 2.— A portion of the FUSE LiF1A spectrum of NGC 3783. Most of the absorption lines in this spectrum are due to molecular hydrogen in the interstellar medium of the Galaxy and the high velocity cloud HVC 287.5+22.5+240. The identifications for these lines are shown at the top of each panel, with the lower set of tick marks indicating absorption at the velocity of the HVC (+240 km s^{-1}). Additional features due to Ar I and Fe II are also indicated. The exposure time for this observation was 37 ksec. The data are binned to a sampling interval of $\approx 8 \text{ km s}^{-1}$ per pixel and have $S/N \approx 10\text{--}15$ per 20 km s^{-1} resolution element.

Fig. 3.— Continuum normalized profiles for selected interstellar lines in the spectrum of NGC 3783. The left panel contains atomic species. Absorption is clearly present in the atomic lines at low, intermediate, and high velocities. The right panel contains various H_2 lines in different rotational levels. Absorption is present at both low and high velocities. The +240 km s^{-1} velocity of the HVC is marked in each panel by the vertical dashed line. When other lines are present in addition to the primary line illustrated, the identifications (without wavelengths) are given above the spectrum.

Fig. 4.— Logarithmic gas-phase abundances for Ar, P, S, Si, and Fe in HVC 287.5+22.5+240. The abundances have been normalized against the Solar System meteoritic values listed in Table 2. Approximate metallicities ($[\text{Fe}/\text{H}]$) derived from stellar/nebular abundances are shown for the LMC and SMC; values of $[\text{O}/\text{H}]$ are about 0.12 dex lower (Russell & Dopita 1992). The HVC data points are compared to the values shown for diffuse clouds in the Galactic halo and the SMC (see text). Note that the HVC metallicity derived from $[\text{S}/\text{H}]$ closely matches that of the SMC.

Fig. 5.— Single-component curve of growth for the H_2 lines identified in the spectrum of NGC 3783 (see Table 1). Data points for rotational levels $J = 0 - 3$ are shown with the symbol coding and the values of N_J indicated in the legend. The dashed lines indicate the curves of growth appropriate for b-values of 10 and 14 km s^{-1} .

Fig. 6.— H_2 column density (N_J) divided by statistical weight (g_J) as a function of excitation energy (E_J) for rotational levels $J = 0 - 4$ in HVC 287.5+22.5+240. The values expected for two different Boltzmann distributions with the temperatures indicated are also shown as dashed lines. Note that there appears to be a clear difference in the slopes of the lines derived from the low- J and high- J lines. The data point for $J = 4$ is a 2σ upper limit. All other errors are 1σ estimates.

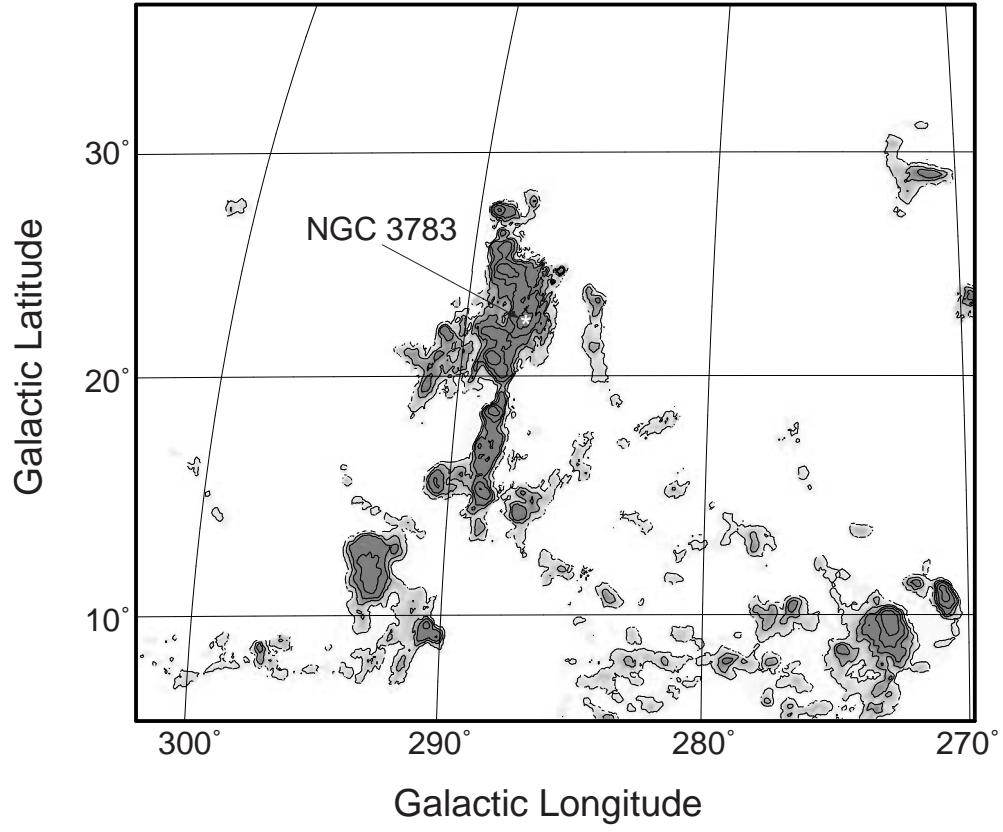


Figure 1.

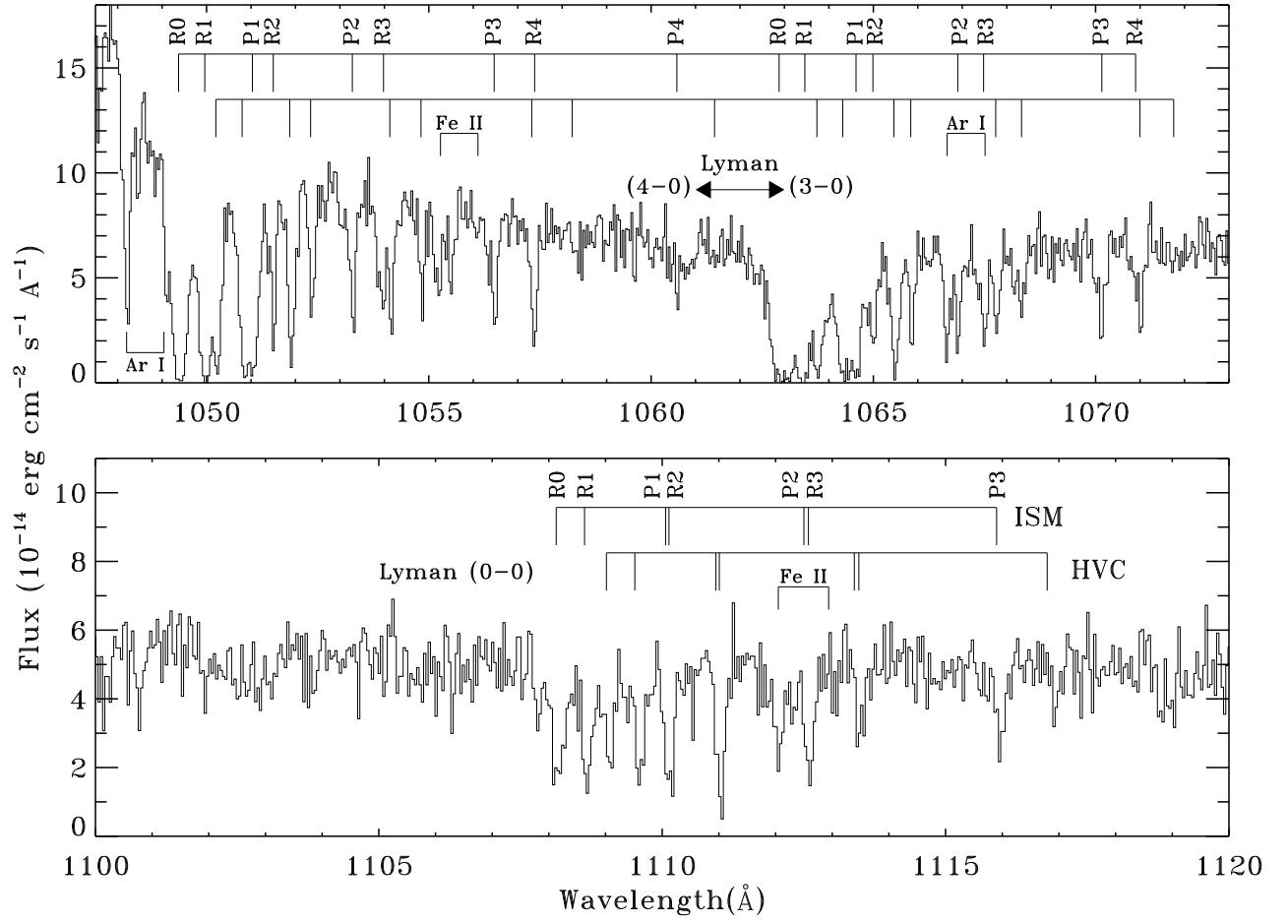


Figure 2.

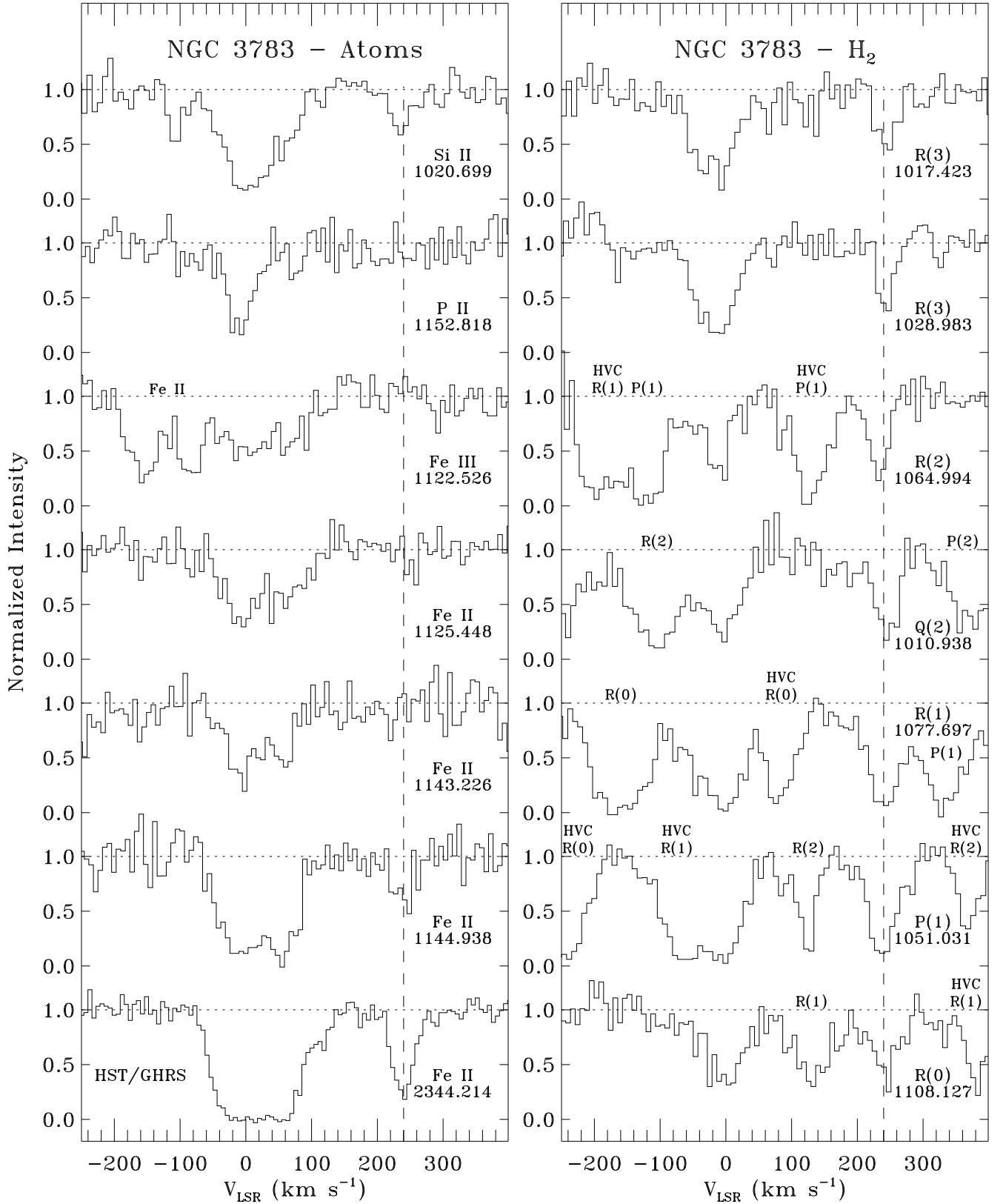


Figure 3.

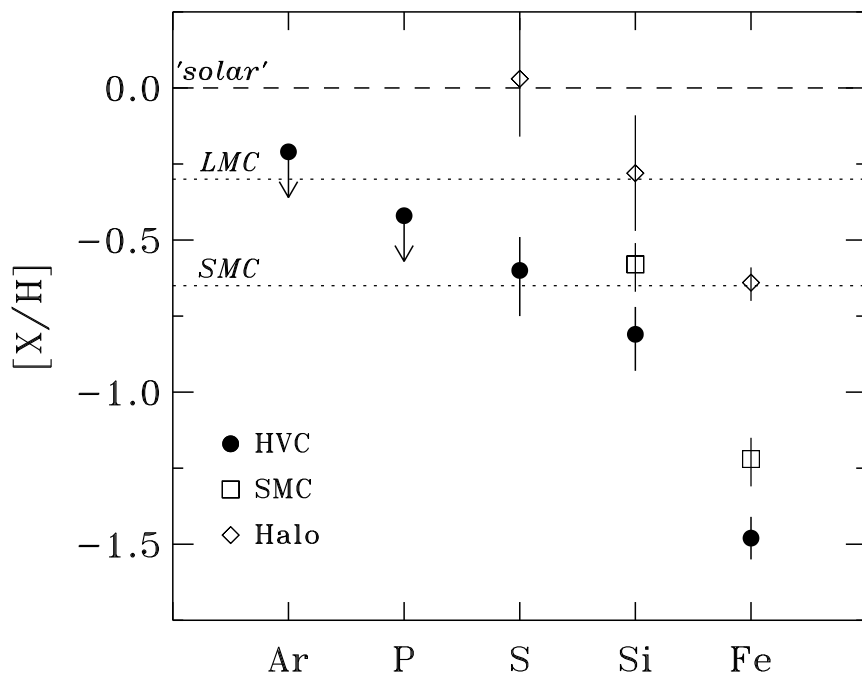


Figure 4.

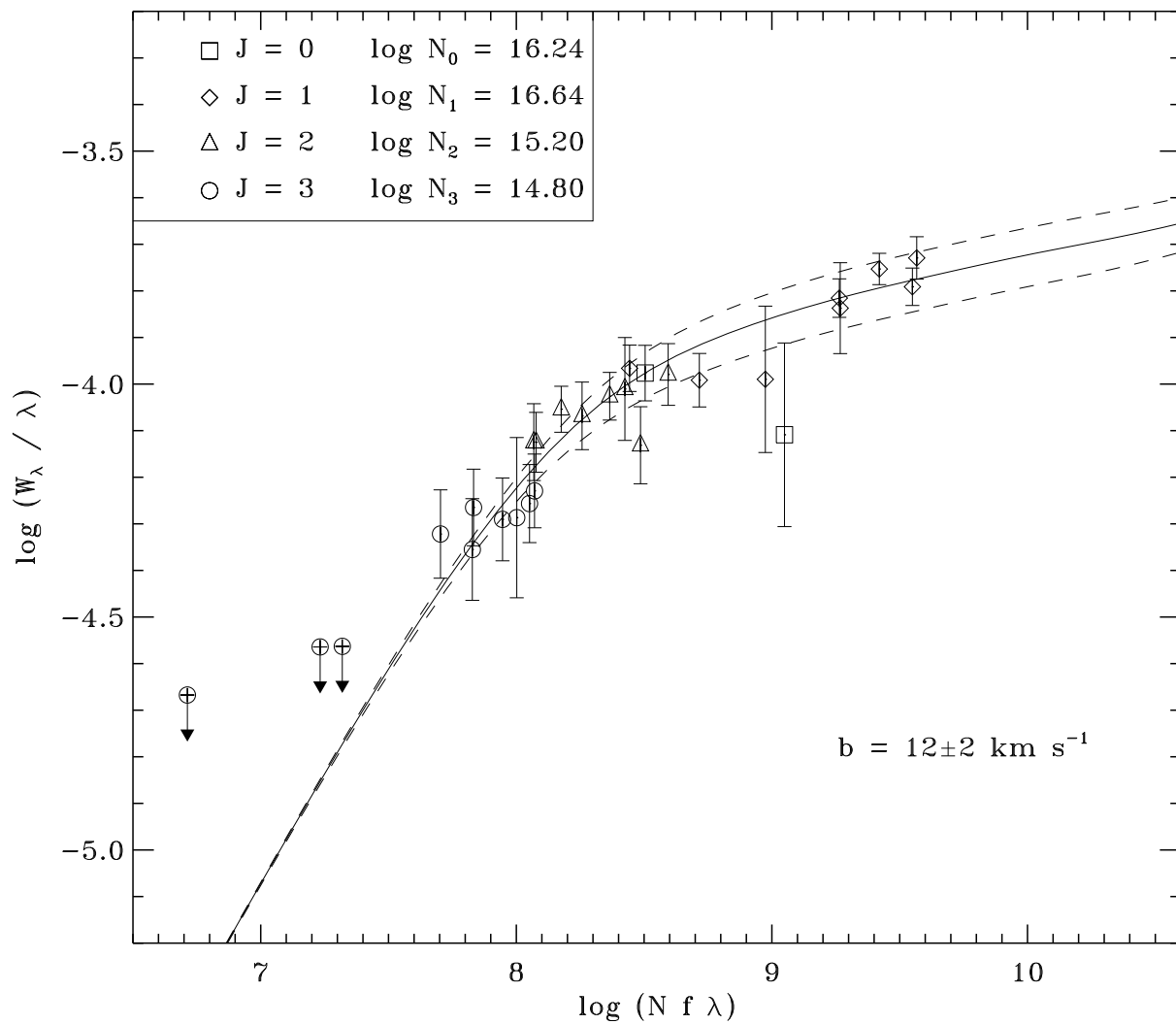


Figure 5.

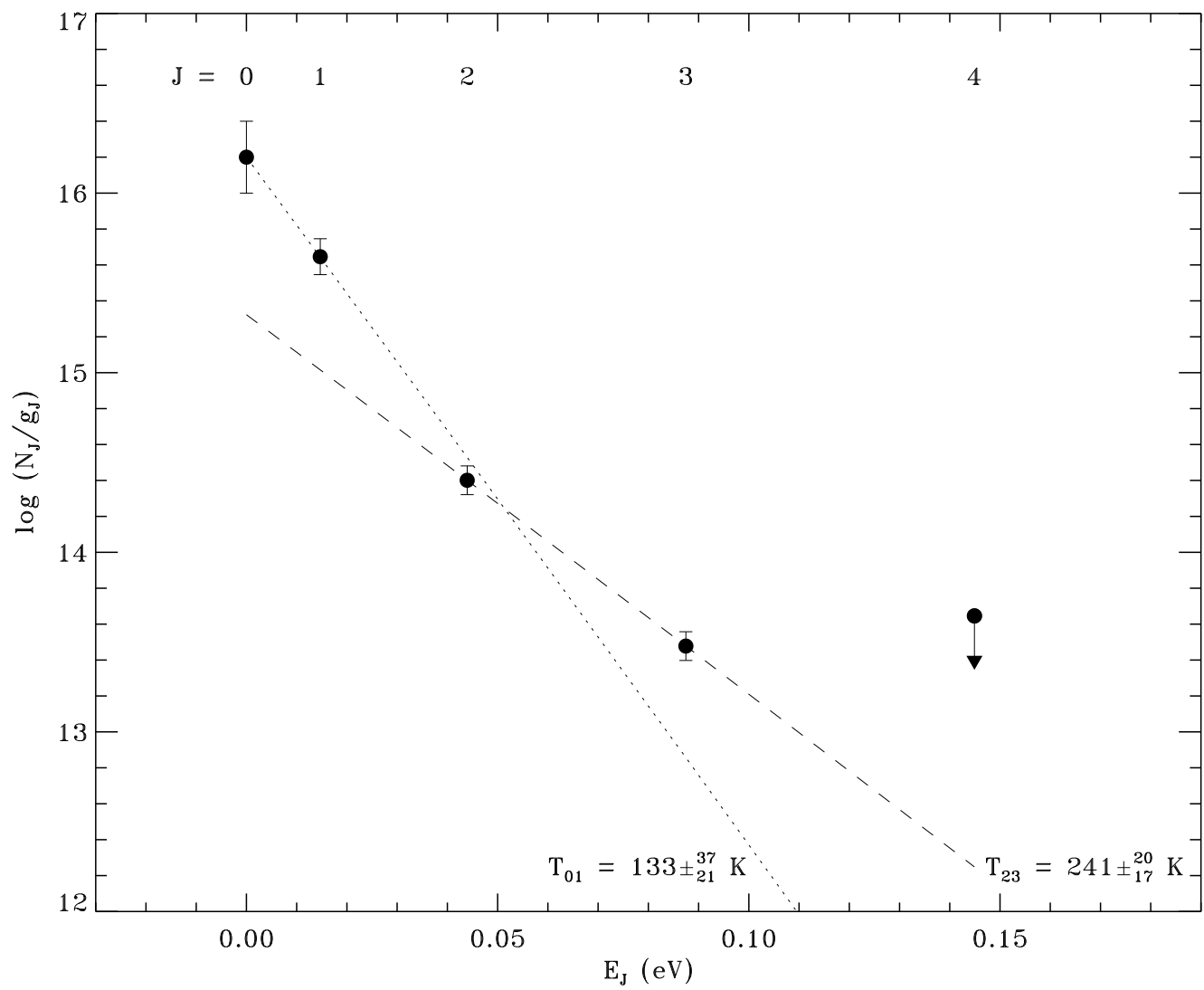


Figure 6.